First-principles study of phonons, optical properties, and Raman spectra in MgV_2O_5

Jürgen Spitaler,[1,2,*] Eugene Ya. Sherman,[2,3] and Claudia Ambrosch-Draxl[1,2]
[1]*Chair of Atomistic Modelling and Design of Materials, Montanuniversität Leoben, Franz-Josef-Straße 18, A-8700 Leoben, Austria*
[2]*Institut für Physik, University Graz, Universitätsplatz 5, A-8010 Graz, Austria*
[3]*Departamento de Química Física, Universidad del País Vasco–Euskal Herriko Unibertsitatea, 48080 Bilbao, Spain*
(Received 19 September 2007; revised manuscript received 25 July 2008; published 19 August 2008)

The electronic properties of MgV_2O_5 are calculated in the framework of the all-electron full-potential linearized augmented plane-wave method within density-functional theory. Adopting the experimental lattice parameters, all atomic positions inside the unit cell are optimized. It is shown that this relaxation has a strong effect on the bond lengths and hence the electronic bands. The optical properties are determined within the independent-particle approximation. In addition, the fully symmetric A_g phonon modes are calculated by the frozen phonon approach. For each eigenvector, the dielectric tensor is obtained as a function of the displacement coordinates. Based on these results, the corresponding Raman spectra are determined and discussed in the context of experimental data. Theory is able to either confirm or revise the assignment of the measured spectra. Finally, the calculated properties are compared with those of other vanadium ladder structures.

DOI: 10.1103/PhysRevB.78.064304 PACS number(s): 71.15.Mb, 63.20.−e, 78.30.−j

I. INTRODUCTION

The magnesium vanadate MgV_2O_5 belongs to the family of vanadium ladder compounds, which has been intensively studied during the last decade. The typical building elements of these materials are ladder-type structures which are arranged in planes. They are formed by V atoms linked via oxygens. The interactions within one ladder are considerably larger than the ones between neighboring ladders of one plane, while in stacking direction only very weak interactions are present. This situation is reflected in a low-dimensional behavior, where the interplay of lattice, charge, and spin degrees of freedom leads to complex physical phenomena. The most prominent member of this family is NaV_2O_5. In this structure, where one electron is shared by the two V atoms of one rung, a spin-Peierls-type transition is encountered,[1–4] which is accompanied by charge ordering.[5–8] In CaV_2O_5, where two electrons per rung are available, no phase transition but a spin singlet state with a gap of 500 K is found.[9] The same is true for the chemically equivalent MgV_2O_5, but the gap is much smaller, i.e., only 15 K,[10,11] which is due to the fact that in MgV_2O_5 the exchange couplings along the leg and along one rung are of comparable strength.[12]

From a structural point of view, MgV_2O_5 is equivalent to NaV_2O_5 and CaV_2O_5 with respect to the ladder planes, but the stacking of these planes differs. While in the latter two compounds the planes are stacked without any shift along z direction, in the magnesium compound the ladders are shifted by half the distance when going from one plane to the next, such that the unit cell is doubled along the stacking direction. In contrast to CaV_2O_5 and especially NaV_2O_5, where a large amount of experimental and theoretical studies has been published, for MgV_2O_5 only few results are available in literature. On the experimental side, structural data,[13,14] magnetic susceptibility,[10,11] and electron-paramagnetic-resonance (EPR) measurements,[10] unpolarized Raman and infrared spectra[15,16] are found. Regarding theory, results for the structure with experimental atomic positions[12,17,18] have been obtained. First results for a relaxed structure have been presented[19] in Ref. 20, however a comprehensive *ab initio* study is still missing.

In this work, we first investigate the lattice relaxation effects on the bond lengths and consequently on the electronic properties and of MgV_2O_5. From the Kohn-Sham band structure, the optical properties are calculated. The Hubbard U parameter for V can be important to understand the behavior of both quarter-filled[21] and half-filled vanadium ladder compounds. However, the magnitude of U in these materials is moderate,[22,23] and even in highly correlated materials such as $YBa_2Cu_3O_7$ vibrational and optical properties are well reproduced by standard density-functional theory (DFT) calculations.[24] In addition, in Ref. 12 the band-structure parameters obtained with the local-density approximation (LDA) and LDA+U calculations were compared and found to be in good agreement. For these reasons we use the LDA rather than the LDA+U method.

The eigenvectors and eigenmodes of the fully symmetric A_g phonon modes are presented in detail. Combining the vibrational properties with the calculation of dielectric tensors as a function of the displacement patterns, the Raman spectra are determined in xx, yy, and zz geometries. Both the peak positions, i.e., the phonon frequencies, as well as the Raman intensities are used to evaluate the assignment of the measured data. The results for MgV_2O_5 are compared with the ones for NaV_2O_5 and CaV_2O_5. Finally, the results are summarized, and some conclusions are drawn.

II. CRYSTAL STRUCTURE AND SYMMETRY

MgV_2O_5 crystallizes in the orthorhombic base-centered space group *Cmnm* (No. 63). It comprises the same rotations as NaV_2O_5 and CaV_2O_5, but the corresponding nonprimitive translations are different. In terms of the Wyckoff positions, V, O2, and O3 have site symmetry 8*f*, while both Mg and the in-rung oxygen O2 reside in 4*c*-type positions. In order to be consistent with the nomenclature used for NaV_2O_5 and CaV_2O_5 with space group 59 (*Pmmn*), we choose x as the

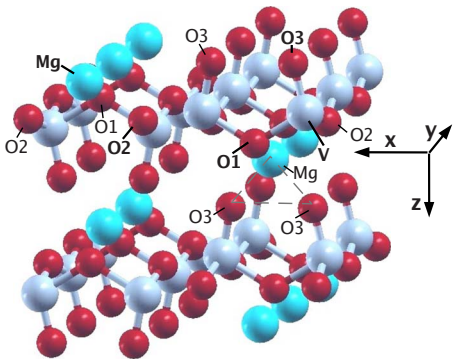

FIG. 1. (Color online) Crystal structure of MgV_2O_5 from a slant perspective (Ref. 25). The triangle indicates the x-z plane that includes both the Mg atom of the upper layer and the two apex oxygens O3 of the lower layer.

direction parallel to the rungs, y parallel to the legs, and z as the stacking direction, which is different from the orientation in Refs. 13 and 14 and consistent with Ref. 16. Moreover, we refer to the in-rung oxygen as O1 and to the apex oxygen as O3, thus swapping the labels with respect to Refs. 13 and 14 where the experimental structure determination is described.

The crystal structure of MgV_2O_5 (Refs. 13 and 14) is presented in Fig. 1. The V-O oxygen layer, together with the metal atom, forms the same geometry as the corresponding building block in NaV_2O_5 and CaV_2O_5. However contrary to them, the crystal has a twice as large period in z direction. This is due to the fact that, going from one x-y plane to the next, the ladders are shifted by $b/2$ with respect to each other. As a consequence, the Mg atom located in the center of two rungs with respect to one ladder lies in the same x-z plane as the apex oxygens (O3) of the neighboring ladder, as it is indicated by the dashed triangle in Fig. 1. This leads to a drastically reduced distance between Mg and O3 (2.06 Å), which is about 20% shorter than the metal-O3 distance in sodium and calcium vanadate. In fact, it hardly differs from the distance between Mg and its nearest neighbor, the in-rung oxygen O1, which is 2.02 Å. Comparing the geometry within *one layer* with the one in NaV_2O_5 and CaV_2O_5, the z coordinates of V and O1 differ considerably more, thus leading to a smaller V-O1-V angle and a noticeably increased V-O1 distance. In turn, Mg is closer to the ladder plane compared to Na or Ca, which implies a decreased distance between the metal ion and O2 (2.24 Å in MgV_2O_5 compared to about 2.50 Å in NaV_2O_5 and CaV_2O_5). The two different V-O2 distances (along one leg and to the leg of the neighboring ladder, respectively), and the distance between V and the apex oxygen, are very similar in all three vanadates.

III. COMPUTATIONAL METHODS

All band-structure calculations have been performed within DFT using the full-potential augmented plane wave +local orbital (FP-APW+lo) (Ref. 26) formalism as implemented in the WIEN2K code.[27] The results presented here have been obtained using the generalized gradient approximation[28] (GGA) for the exchange-correlation (xc) effects; we will come back, however, to the influence of the particular choice of the exchange-correlation potential in Sec. V. The atomic sphere radii R_{MT} were chosen as 1.6 a.u. for V, 1.5 a.u. for Mg, and 1.4 a.u. for the O atoms. For the wave functions, a plane-wave cutoff $K_{max}=4.64$ was used in all calculations, which implies $R_{MT}\times K_{max}$ values of 6.5 for O, 6.96 for Mg, and 7.43 for V. We used 300 **k** points in the full Brillouin zone (BZ) for the self-consistency cycles and 7569 **k** points for the calculation of the dielectric functions. The plane-wave cutoff for expanding the charge density and potential in the interstitial region, G_{max}, was 14. All atomic positions have been relaxed, i.e., the atoms were shifted from the experimentally measured ones[13] until the forces were smaller than 1 mRy/a.u.

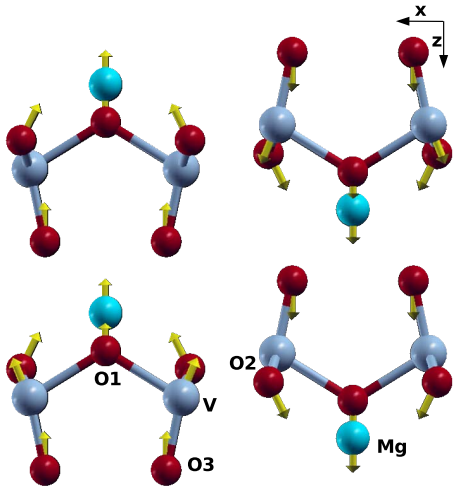

FIG. 2. (Color online) Relaxation-induced shifts of the atomic positions (magnified by a factor of 5). The labeled sites represent the reference atoms for Table I.

IV. RESULTS

A. Crystal structure

The changes in the atomic positions due to relaxation are shown in Fig. 2 and Table I. In general, all atoms of one ladder are simultaneously moved in z direction by more than 0.15 Å, while the neighboring ladder in the same plane is moved against it due to symmetry. The shift of the in-rung oxygen O1 parallel to z is about 0.02 Å smaller compared to the displacements of the V atoms resulting in a flattened V-O1-V angle. At the same time, the displacement of the V atoms exhibits an x component ($|\Delta x|=0.075$ Å), such that the V-O1 distance is increased by 0.052 Å. In other words, the rungs of the ladders are stretched. Concerning the legs, the V-O2-V kink is slightly weakened, since the V-O2 distance is reduced by 0.012 Å. At the same time, the interladder distance, i.e., the distance between the V and the O2 atom of the neighboring leg, is reduced by about 0.02 Å. The apex oxygen O3 is shifted in the same direction as the vanadium atom, but its x component stays almost the same, which results in an increase in the V-O3 bond length by 0.01 Å. The displacement of the Mg atoms is smaller than the one of the apex O3, which is the closest neighbor belong-

TABLE I. Shifts of the atoms from the experimental positions (upper panel) and changes in interatomic distances d (lower panel) due to relaxation. The left column of the upper panel shows the representative atom of each atom type which the shift in the right column refers to.

Reference atom	$(\Delta x, \Delta y, \Delta z)$ (Å)
V (0.5970, 0, 0.7981)	(–0.075, 0, –0.179)
Mg (0.2500, 0, 0.8868)	(0.000, 0, 0.174)
O1 (0.7500, 0, 0.6956)	(–0.004, 0, –0.185)
O2 (0.4205, 0, 0.7642)	(–0.086, 0, 0.170)
O3 (0.6285, 0, 0.9568)	(0.000, 0, –0.154)

	Δd (Å)
V-O1	0.052
V-O2 (same leg)	–0.012
V-O2 (neighbor leg)	–0.018
V-O3	0.010
Mg-O1	0.008
Mg-O3	0.011

ing to the next ladder in stacking direction, such that the distance between these two atoms is increased by 0.01 Å. The same holds for the Mg-O1 distance, since, compared to the metal atom, O1 is less affected by the relaxation.

B. Electronic properties

The lower part of Fig. 3 shows the band structure and atomic densities of states (DOSs) of MgV_2O_5 for the relaxed (upper panel) and experimental[13] (lower panel) atomic positions. The **k** path for both band-structure plots is visualized in the upper part of the same figure. In order to facilitate comparison with the results for NaV_2O_5 and CaV_2O_5, a path analogous to the one in Ref. 22 is used. The symmetry-projected densities of states for the relaxed structure are plotted in Fig. 4. Generally, the highest valence bands consist of the bonding pair of V $3d_{xy}$ levels, while their antibonding counterpart is found above the Fermi level, as already described in Ref. 12. In the bands next higher in energy, admixtures of V $3d$ levels with different orbital characters are found, where also the apex oxygen O3 contributes. The lower-lying valence bands, i.e., 2–3 eV below the V $3d_{xy}$ levels, are mainly formed by the in-rung oxygen p_x, the in-leg oxygen p_y, and O3 p_x orbitals.

The relaxation of the atomic positions has a large impact on the details of the band structure. The experimental atomic positions result in a splitting between the V $3d_{xy}$ orbital and the other V $3d$ levels, which is so pronounced that the xy bands are completely separated from the rest.[12] Upon relaxation not only the splitting is removed but the V $3d_{xy}$ levels considerably overlap with the xz and yz bands (Fig. 4). While for the experimental structure the antibonding V $3d_{xy}$ bands are located at the Fermi level and attached to the bonding ones, in the relaxed structure they are completely detached from their bonding counterparts and strongly overlap with

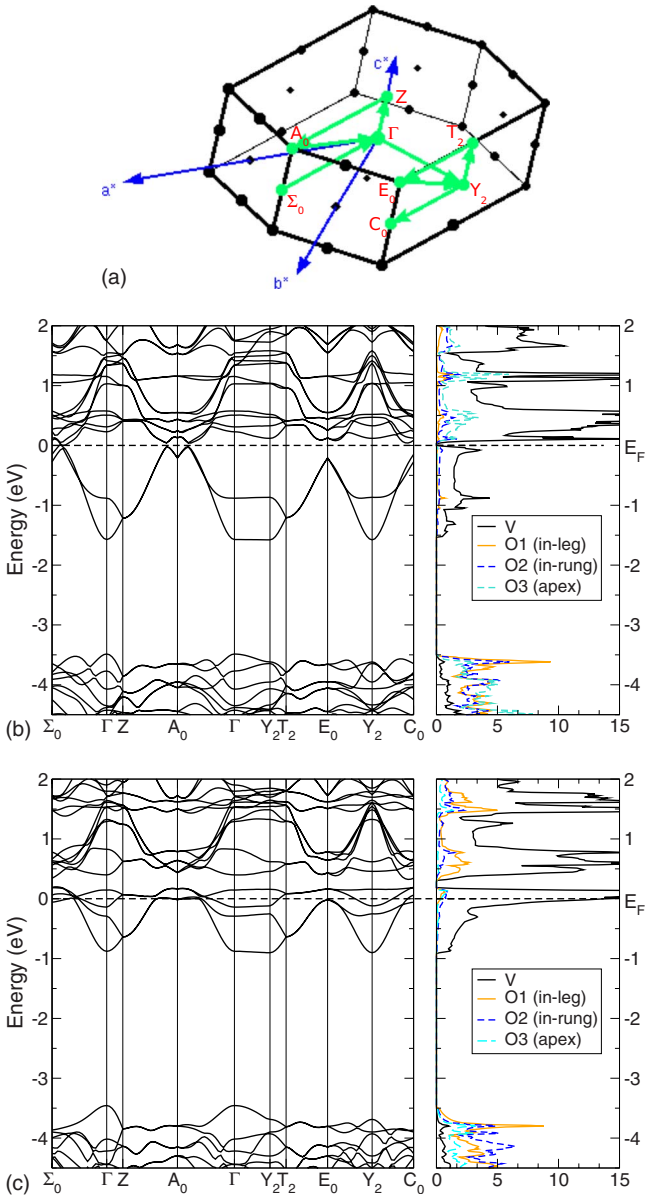

FIG. 3. (Color online) Upper part: Brillouin zone and **k** path used for the band-structure plot. Lower part: band structure and atomic densities of states (in states per eV and unit cell) for relaxed (upper panel) and experimental (Ref. 13) atomic positions (lower panel).

the conduction bands next higher in energy. As a consequence, the DOS vanishes at E_F, in contrast to the nonrelaxed situation, where a large DOS at the Fermi level is found.[13] Together with this shift, the bandwidth and dispersion of the antibonding V $3d_{xy}$ bands change drastically. While for the experimental geometry these bands are rather flat and the bandwidth is only about 0.3 eV, Figs. 3 and 4 show that in the relaxed structure they are much more dispersive and spread over a range of more than 0.7 eV. A big change in bandwidth is also detected for the bonding V $3d_{xy}$ levels just below E_F. While for the unrelaxed structure it is about 1 eV, the relaxation causes a larger overlap of the V $3d_{xy}$ orbitals with the p_x levels of the O2 atoms on the same leg, which leads to an increased bandwidth by roughly

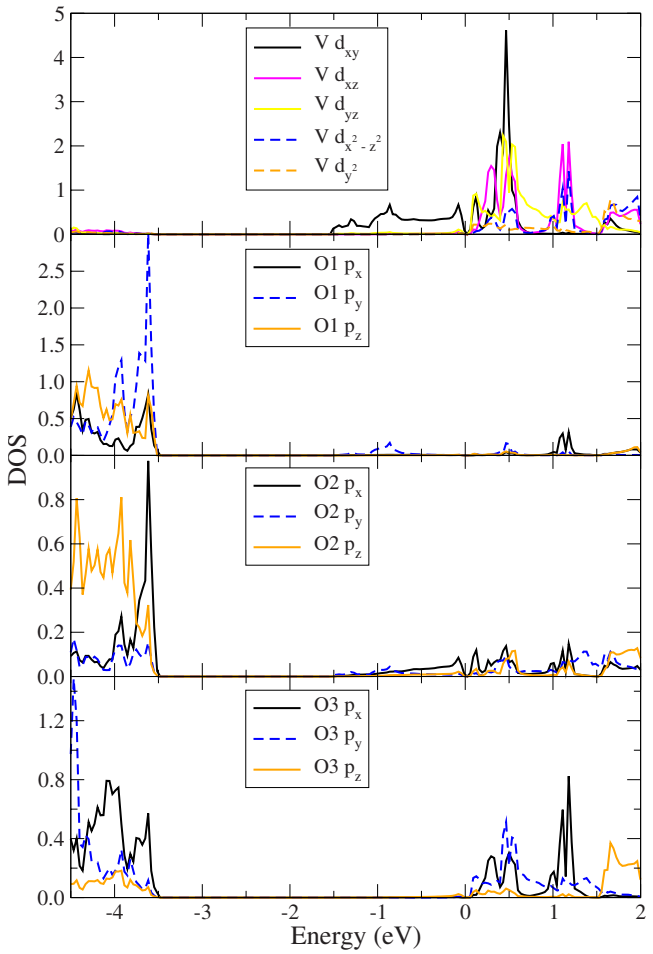

FIG. 4. (Color online) Partial densities of states (states per eV and atom) of the relaxed structure, showing the orbital character of the V $3d$ and the O $2p$ bands. In the considered energy range no magnesium states are present.

50%. Nevertheless, the splittings at Γ and Z change rather little. Also the O $2p$ dominated bands 4 eV below E_F are affected by the structure relaxation. The dispersion gets weaker, while between Σ_0 and Γ a crossing of the two O $2p$ bands highest in energy is detected. However, the maximum of the O $2p$ bands can be found at almost the same energy for either case.

C. Optical properties

The dielectric tensor components for the relaxed structure of MgV_2O_5 are presented in Fig. 5. They are obtained from the Kohn-Sham eigenvalues within the independent-particle approximation using a lifetime broadening of 0.1 eV. Thereby, the real part, Re $\varepsilon_{ii}(\omega)$, is obtained by Kramers-Kronig transformation from the imaginary part, Im $\varepsilon_{ii}(\omega)$. Details of the method are presented in Ref. 29.

Since there is only a small gap between bonding and antibonding bands in MgV_2O_5, large contributions to all three components at energies below 0.5 eV are found. Moreover, in Im ε_{xx} there is a pronounced feature at 1.25 eV, and a weaker shoulder at 1.7 eV appears. While the former can be

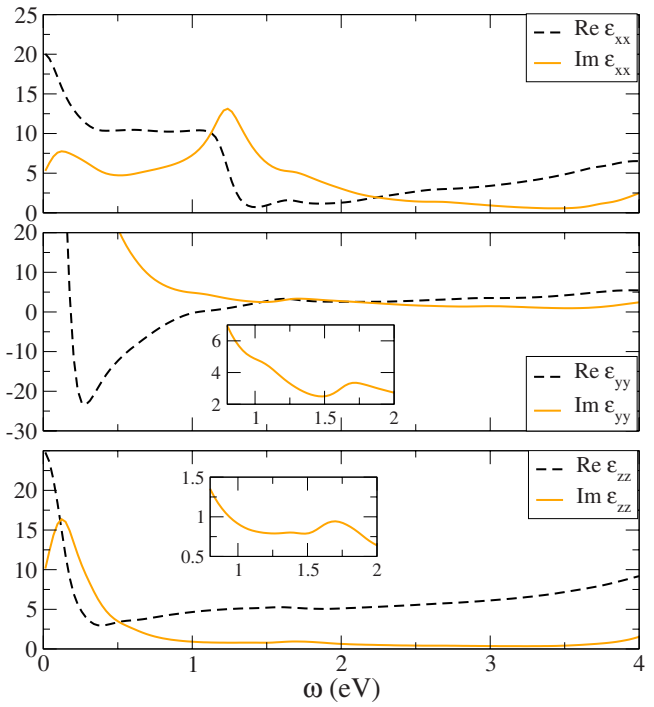

FIG. 5. (Color online) Real and imaginary parts of the dielectric function of MgV_2O_5 in xx, yy, and zz polarizations.

assigned to bonding→antibonding transitions around the Γ point, the latter corresponds to transitions from the bonding V $3d_{xy}$ bands to V $3d_{xz}$ at about 1.2 eV (see Fig. 4).

In ε_{yy}, the peak below 0.5 eV is strongly dominating. Yet, a slight shoulder at 1.1 eV and a peak at 1.7 eV can be detected. As in the case of the xx component, the first feature can again be assigned to transitions from bonding to antibonding V d_{xy} levels around the Γ point, and the 1.7 eV peak represents excitations between the V $3d_{xy}$ and V $3d_{xz}$ bands as described above. Regarding the zz component, in the frequency range above 0.5 eV no peaks can be distinguished, except for a weak feature at 1.7 eV, which has the same origin as its counterparts in xx and yy polarizations.

D. A_g phonon modes

On the experimental side, only Raman spectra with unpolarized laser light are available,[15,16] such that the calculated peak positions, i.e., phonon frequencies, together with the Raman intensities facilitate the symmetry assignment of the measured data. The factor group analysis for the MgV_2O_5 structure yields, after subtraction of three acoustic ($B_{1u}+B_{2u}+B_{3u}$) and three silent A_u modes,

$$\Gamma = 8A_g(xx,yy,zz) + 3B_{1g}(xy) + 8B_{2g}(xz) + 5B_{3g}(yz) + 7B_{1u}(\mathbf{E}\parallel\hat{z}) + 4B_{2u}(\mathbf{E}\parallel\hat{y}) + 7B_{3u}(\mathbf{E}\parallel\hat{x}), \quad (1)$$

i.e., there are 24 Raman active (all "gerade" modes) and 18 infrared-active (B_{nu} species) phonon modes, where the letters in parentheses indicate the polarization of the incoming and outgoing light, respectively. The 8 degrees of freedom contributing to the eight Raman-active A_g modes comprise the x and z coordinates of V, the in-rung oxygen O2, and the apex

oxygen O3, respectively, together with the z coordinates of Mg and O1. The phonon eigenfrequencies and eigenvectors of the A_g modes are determined in the so-called *frozen-phonon* approximation, where we consider for each participating degree of freedom four displacements, two in positive and two in negative direction. Details about the procedure can be found, for example, in Ref. 24.

The eigenvectors $\mathbf{e}_{\alpha\zeta}$ are normalized with respect to the primitive unit cell, including 2 formula units of MgV_2O_5, such that

$$\sum_{\alpha=1}^{N} \mathbf{e}_{\alpha\zeta}^2 = 1, \tag{2}$$

where α enumerates the ions, $N=16$ is the number of ions per primitive unit cell, and ζ indicates the phonon mode. For each set of equivalent atoms only the components corresponding to one atom are reported where this reference atom is highlighted in the 1019 cm^{-1} mode of Fig. 6 using bold characters.

The eigenvectors and eigenfrequencies of MgV_2O_5 are shown in Table II and Fig. 6, respectively. Although the Raman spectra will be presented in detail in Sec. IV E, some of them are required for the analysis of experimental peak positions and hence are already discussed to some extent at this point. In Refs. 15 and 16 phonons were studied with unpolarized Raman scattering, and, therefore, no phonon symmetry could be obtained from the experimental data directly. In Ref. 16 a total of 15 Raman peaks were observed and interpreted in terms of symmetry and eigenvectors by comparison to polarized scattering results on NaV_2O_5. Eight of the measured peaks were attributed to the A_g modes. However, our calculations imply a different assignment for some of the modes. Hence, for this reference, a second column is added (marked by *), which contains our assignments of the A_g modes from the set of peaks measured by Popović *et al.*[16]

The frequency of the V-O3 stretching mode (1019 cm^{-1}) excellently agrees with experiment, and also the assignment is unambiguous. It represents a stretching of the strongest bond, i.e., the bond between V and the apex oxygen O3. Also the 546 cm^{-1} mode is very close to the experimental frequency, but the experimental assignment is not verified. While in NaV_2O_5—which is the reference material for the assignment in Ref. 16—the mode with the second highest frequency can be identified as a V-O2 stretching, in MgV_2O_5 the main feature of the 546 cm^{-1} mode is rather an in-phase motion of the V and O2 atoms of one leg in x direction, while the two legs of one ladder vibrate against each other and the leg of the next neighboring ladder. In addition, each leg shows a zigzaglike deformation in the x-y plane due to the fact that the O2 atom is shifted more strongly than the V atom. Also for the 419 cm^{-1} mode, the experimental assignment has to be revised. Instead of a pure V-O1-V stretching, which is encountered in NaV_2O_5,[16,23] in MgV_2O_5 this mode represents a more complex vibration, with O2 moving in z direction, out of phase with respect to the neighboring V, while O3 has a considerable component parallel to the V motion. In other words, the V-O3 moiety moves as a whole against the leg and rung oxygens. Correspondingly, the frequency differs considerably from its counterpart in NaV_2O_5.[16,23] In turn, the peak measured at 478 cm^{-1}, which was also interpreted as A_g mode in Ref. 16, must stem from a phonon mode with other symmetry. The 395 cm^{-1} mode of MgV_2O_5, in turn, is comparable with the O 1_z+O2−V−O3 mode found in NaV_2O_5,[16,23] also exhibiting an O2-V-O3 bending. However, the in-rung oxygen O1 hardly participates in this eigenmodes, while Mg has a considerable z component.

The 353 cm^{-1} mode of MgV_2O_5 represents an out-of-phase vibration of the in-rung O1 and the in-leg O2 in z direction, while the V atoms virtually stay at their positions. Instead, the Mg atoms are displaced parallel to the O2 atoms

TABLE II. Calculated eigenfrequencies (cm^{-1}) and eigenvector components of the A_g phonon modes compared to experimental results from literature. The frequencies in the column of Ref. 15 are selected from the unpolarized spectra by comparison with theory, such as the ones of Ref. 16 marked by *, while the column left of it shows the results directly as they are presented in the same reference. Details are explained in the text.

Experiment				Theory									
Assignment	ω (cm^{-1})			ω	Eigenvector								Assignment
Ref. 16	Ref. 15	Ref. 16	Ref. 16*	(cm^{-1})	V_x	V_z	Mg_z	$O1_z$	$O2_x$	$O2_z$	$O3_x$	$O3_z$	
V-O3 stretch.	1001	1002	1002	1019	−0.07	0.23	0.01	0.01	0.01	0.01	−0.13	−0.42	V-O stretch.
V-O2 stretch.	534	536	534	546	0.13	−0.07	−0.01	0.05	0.46	−0.11	0.02	−0.04	Leg↔leg
V-O1-V bend.	413	478	414	419	0.10	0.16	−0.13	−0.36	0.11	0.33	0.12	0.09	$O2_z$+V−O1−V bend.
O-V-O bend.	373	414	374	395	0.33	0.17	0.17	0.00	−0.05	0.03	−0.30	−0.05	Mg_z+O3−V−O2 bend.
O-V-O bend.	314	?	315	353	0.01	−0.06	−0.21	−0.36	−0.06	−0.34	−0.16	−0.10	O2-V-O1 bend.
O-V-O bend.	278 (299?)	233	278 (300.5?)	310	−0.34	0.14	0.30	−0.15	0.14	−0.03	−0.16	0.08	Mg_z+O1−V−O3 bend.
Mg‖c	219		220	250	0.17	−0.02	0.31	−0.15	−0.08	−0.19	0.34	0.06	Mg_z+O1−V−O3 breath.
chain rot.	98	98	98	104	0.00	0.37	−0.15	0.12	0.01	−0.20	0.07	0.23	chain rot.

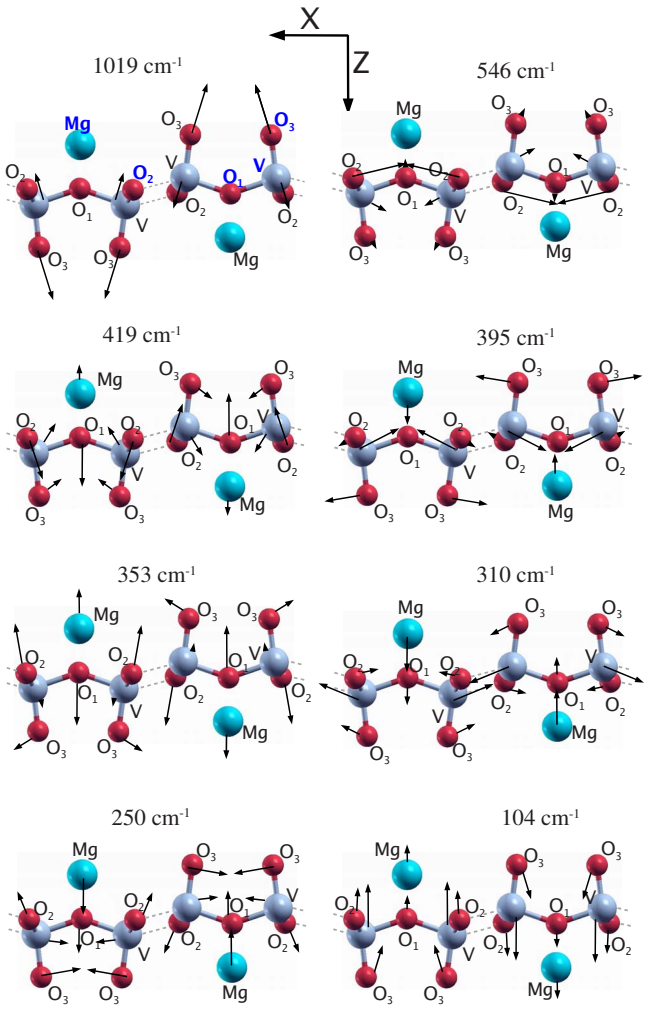

FIG. 6. (Color online) A_g phonons of MgV_2O_5. The arrows show the eigenvectors for each eigenmode, i.e., the direction and magnitude of the atomic displacements weighted by the square root of the corresponding atomic mass.

of the same ladder, while the eigenvector components of the apex oxygen moving perpendicular to the V-O3 bond is comparatively small. The involvement of Mg on the one hand and the minor participation of O3 and V on the other hand are the main differences to the corresponding eigenmode[16,23] of NaV_2O_5 at 308 cm^{-1}, which has pronounced O2-V-O3-bending character. In Ref. 16, there is no such A_g mode identified for MgV_2O_5, even though there is a peak found at 315 cm^{-1}. Comparison to the theoretically obtained frequencies and the Raman spectra make it very probable that the peak at 315 cm^{-1} has A_g symmetry, both, due to its position and its intensity. Hence this peak was included in Table II. The symmetry assignment made in Ref. 16 may have to be revised also for the A_g mode at 310 cm^{-1}. First, the theoretically obtained frequency shows that there must be an A_g mode considerably higher in frequency than 233 cm^{-1}. Second, the Raman spectra presented in Sec. IV E clearly show that the corresponding peak must have strong intensity, while the peak at 233 cm^{-1} in Ref. 16 is rather weak. For these reasons we claim that not the 233 cm^{-1} but more probably the 278 cm^{-1} peak corresponds to the theoretically found A_g mode at 310 cm^{-1}. Another candidate could be an experimental peak at 300 cm^{-1}, which is closer in frequency, but its low intensity is inconsistent with the theoretical findings and suggests that it may stem from some B_{ng} mode. The 310 cm^{-1} mode represents an O1-V-O3 bending, where Mg vibrates in phase with the apex oxygen O3. Since also the O2 atoms contribute to this eigenmode, it has a certain similarity to the O2-V-O3 bending mode of NaV_2O_5 (Refs. 16 and 23) at 232 cm^{-1}.

The MgV_2O_5 A_g mode second lowest in frequency at 250 cm^{-1}, in contrast, deviates strongly, both, in frequency as in the eigenvector components, from its counterpart in NaV_2O_5. Instead of representing a vibration of the metal ion against the rest of the ladder, in MgV_2O_5 the Mg ion moves in phase with its nearest neighbor, i.e., the in-leg oxygen O1 (see Fig. 6). The most characteristic feature of this mode is a breathing of the pentagon formed by the in-leg oxygen together with the two adjacent V atoms and their apex oxygens. The O2 atoms, in contrast, move out of phase with respect to the rest of the ladder. These two features explain the relatively high frequency of this mode. The assignment of the lowest-frequency mode at 104 cm^{-1}, finally, is unambiguous. Analogous to NaV_2O_5 (Refs. 16 and 23) it can be described as chain rotation mode, where neighboring ladders vibrate antisymmetrically in z direction. The higher frequency of this phonon mode compared to the chain rotation in NaV_2O_5, which has an experimental frequency of 90 cm^{-1}, is due the stronger interladder interaction, which is also reflected in the smaller interladder distance in MgV_2O_5.

E. Raman spectra

The calculated Raman spectra for the A_g modes of MgV_2O_5 at a photon energy of 2.41 eV (514 nm) are presented in Fig. 7 (upper three panels), while unpolarized measurements[16] for the same laser frequency are shown in the lowest panel of the same figure. In the zz polarized spectra the eigenmode highest in frequency predominates strongly, even though also the other eigenmodes can, at least, be distinguished. In yy polarization the 310 cm^{-1} mode, representing a $Mg_z+O1-V-O3$ bending, shows the largest intensity, followed by the chain rotation mode at 104 cm^{-1}, the leg$\leftrightarrow$leg vibration at 546 cm^{-1}, and a second bending mode at 250 cm^{-1}. However, also the modes at 353, 395, and 419 cm^{-1} contribute considerably, while the 1019 cm^{-1} mode is not present in this polarization.

The xx polarized Raman spectra appear to be comparatively balanced in terms of the individual peak heights, i.e., all eight A_g modes can clearly be distinguished. The intensities of the 104 cm^{-1} mode, the 1019 cm^{-1} vibration, and the modes between 350 and 450 cm^{-1} are very similar. The 546 cm^{-1} mode gives a rather weak contribution, whereas the two $Mg_z+O-V-O$ bending modes at 250 and 310 cm^{-1}, respectively, stick out of the rest.

On the experimental side,[15,16] the Raman spectra were obtained using an Ar^+ laser with the photon energy of 2.41 eV (514 nm). The same energy is taken for the theoretical spectra shown in Fig. 7. As mentioned in Sec. IV D, Ref. 15 does not assign any symmetry species to the peaks, while the

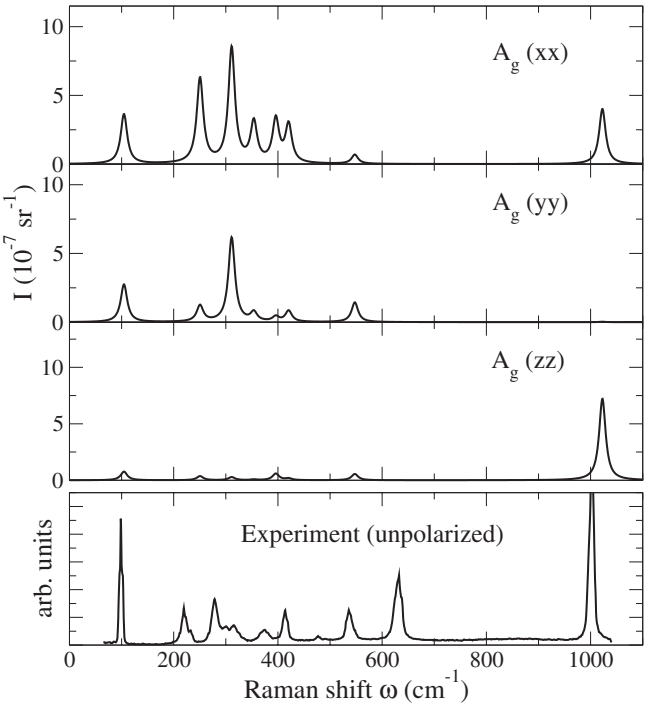

FIG. 7. Theoretical Raman spectra for the A_g modes of MgV_2O_5 for *xx*, *yy*, and *zz* polarizations (upper three panels), compared to unpolarized Raman spectra from experiment (Ref. 16) (lower panel). In the latter, the A_g spectra are superposed by the B_{1g}, B_{2g}, and B_{3g} modes. All results are obtained for a photon frequency of 2.41 eV (488 nm).

assignment in Ref. 16 is done by relating each MgV_2O_5 peak to the polarized NaV_2O_5 peak closest in frequency. Thus, theory improves the interpretation of the experimental spectra. As discussed in Sec. III, the theoretical results imply that the measured peaks[16] belonging to the A_g species are the ones at 1002, 536, 414, 374, 315, 278, 220, and 98 cm^{-1}. In terms of frequency, instead of the 278 cm^{-1} peak another peak at 300 cm^{-1} would be a better candidate for an A_g mode, since theory predicts a peak at 310 cm^{-1}. However, the low intensity of the latter is in contrast to the calculated Raman spectra. Thus we believe that the measured 278 cm^{-1} peak is the one originating from an A_g mode. Regarding the weak peaks at 233 and 478 cm^{-1}, which are assigned A_g species in Ref. 16, our results suggest that they belong to a species other than A_g.

In order to investigate the resonance behavior of the A_g eigenmodes the derivative of the dielectric function with respect to phonon distortions, $|d\varepsilon_{ii}/dQ|^2$, is presented in Fig. 8. As it is the case for NaV_2O_5, also in MgV_2O_5 the *zz* component is considerably affected only by the V-O3 stretching mode at 1019 cm^{-1} and is therefore omitted in the other plots. For this mode $|d\varepsilon_{zz}/dQ|^2$ increases almost linearly with the photon energy (top left in Fig. 8).

The *xx* component of the Raman spectra generally tends to resonate at photon energies less than 2.25 eV. Nevertheless, the 419 cm^{-1} mode deviates from this tendency, exhibiting large values of $|d\varepsilon_{xx}/dQ|^2$ for the whole energy range from 2.2 to 2.8 eV. Moreover, the bending modes at 250 and 353 cm^{-1} show a second resonance at a photon energy of

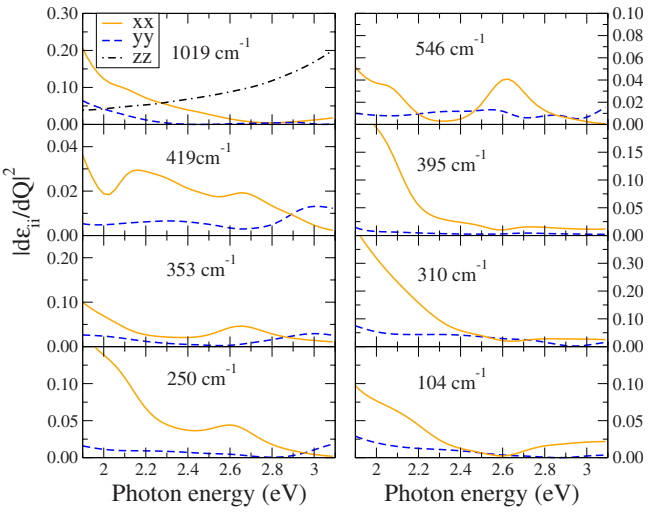

FIG. 8. (Color online) Change in the dielectric function with respect to displacements along the eigenvectors, $|d\varepsilon_{ii}/dQ|^2$, for the A_g eigenmodes of MgV_2O_5.

about 2.6 eV, which is even more pronounced in the leg↔leg vibration with 546 cm^{-1}. Finally, also the chain rotation mode cm^{-1}, where $|d\varepsilon_{xx}/dQ|^2$ is in general comparatively small, shows a minor resonance at about 3 eV. For many phonon modes (1019, 395, and 310 cm^{-1} modes) $|d\varepsilon_{xx}/dQ|^2$ is rather small at the photon energy of 2.44 eV used in the experiments.[15,16] It even has minima for the vibrations of 546, 353, 250, and 104 cm^{-1}. Instead, all modes exhibit resonances at lower photon energies, and some of them at about 2.6 eV, as mentioned just above.

The *yy* component responds rather weakly to any photon energy in the considered range, thus the maxima of $|d\varepsilon_{xx}/dQ|^2$ are by a factor of 5 smaller than the ones in *xx* polarization. A general trend for all A_g modes can hardly be identified. While the eigenmodes with 353, 419, and 546 cm^{-1} show resonances at energies greater than 2.75 eV, the largest values of $|d\varepsilon_{yy}/dQ|^2$ in the 104, 310, and 1019 cm^{-1} vibrations are found at low photon frequencies, respectively, while the modes with 250 and 395 cm^{-1} do not significantly alter ε_{yy} in the whole energy range between 2 and 3 eV. In the 546 cm^{-1} phonon mode, one more noticeable feature is present, namely, a broad maximum of $|d\varepsilon_{yy}/dQ|^2$ centered at a photon energy of about 2.55 eV, with a shoulder at 2.3 eV.

V. DISCUSSION

A. Comparison to NaV_2O_5 and CaV_2O_5

The most striking difference to NaV_2O_5 in the band structure is certainly the shift of the Fermi level up to the top of the bonding V $3d_{xy}$ levels due to the additional valence electron provided by Mg. The width of these bands is about 1.5 eV in MgV_2O_5, while it is less than 1 eV in NaV_2O_5. Moreover, the splitting at the Γ point is almost twice as large in the former. In NaV_2O_5 the antibonding V $3d_{xy}$ bands are clearly separated from their bonding counterparts and from the V $3d_{xz}$ dominated bands higher in energy. In MgV_2O_5

there is a zero gap and all V 3*d* levels overlap considerably. The separation between the vanadium bands at the Fermi level and the oxygen dominated bands around −4 eV is slightly smaller in MgV_2O_5, where it is only 2 eV, compared to approximately 2.5 eV in NaV_2O_5. Most of these findings are a consequence of the structural relaxation, which also causes a crossing of the oxygen bands at −4 eV between Σ_0 and Γ as well as between A_0 and Γ, similar to the situation in NaV_2O_5.[22] The most significant differences in the chemically equivalent CaV_2O_5 are the much smaller bandwidth of the pair of V $3d_{xy}$ bands below E_F and the finite gap.

Concerning the phonon modes, there are considerable differences comparing MgV_2O_5 with sodium and calcium vanadates.[22] First, Mg participates in six of the A_g modes, while in the other two compounds the metal atom contributes to the two vibrations lowest in energy only. Second, some of the low-energy vibrations differ clearly from their counterparts in NaV_2O_5 and CaV_2O_5 in terms of their eigenvectors and have much smaller frequencies. For example, the A_g mode second lowest in frequency exhibits a completely different displacement pattern. In contrast to NaV_2O_5 and CaV_2O_5, where this mode consists of a vibration of the metal atom out of phase with the rest of the ladder, in MgV_2O_5 Mg moves in phase with the in-rung oxygen O1, but the V-O1-V rung together with the apex oxygens show a breathinglike behavior. This goes along with an eigenfrequency increase of about 40%, i.e., 250 cm^{-1} compared to 176 cm^{-1}.

In terms of the Raman spectra, MgV_2O_5 is distinguished from the other two ladder structures especially through the much higher peak of the chain rotation mode with about 100 cm^{-1}. While in NaV_2O_5 and CaV_2O_5 this feature is hardly visible in any polarization, in the case of MgV_2O_5 its contribution is comparable with the largest peaks for *xx* and *yy* polarized lights. The V-O3 stretching mode, which is the A_g vibration highest in energy, appears in *xx* and *zz* polarizations, in contrast to NaV_2O_5, where its peak is very pronounced in all three polarizations, and CaV_2O_5, where it is only present for incoming and outgoing photons polarized in *z* direction. The general shape of the MgV_2O_5 spectra for *yy* polarization is strongly dominated by the contribution from the A_g mode with 310 cm^{-1}, which is not the case in the other two vanadates. The theoretical Raman spectra for *zz* polarized light are very similar for all three compounds, with the contribution of the V-O3 stretching mode 1 order of magnitude larger than all the other peaks.

The resonance behavior of the MgV_2O_5 Raman spectra is similar to that of NaV_2O_5 and CaV_2O_5 with respect to the *zz* component, where $|d\varepsilon_{zz}/dQ|^2$ is tiny for all but not in the V-O3 stretching mode. For *yy* polarized light, the change in the dielectric function with atomic displacements is smaller in MgV_2O_5 than in the sodium and calcium compounds. While in the latter two for some modes $|d\varepsilon_{yy}/dQ|^2$ is comparable to $|d\varepsilon_{xx}/dQ|^2$, for the former it is in general 1 order of magnitude smaller. While NaV_2O_5 exhibits strong resonances for the low-energy range and CaV_2O_5 shows a strong response to photon frequencies of about 2.75 eV, for MgV_2O_5 no general trend is observed.

B. Role of the exchange-correlation potential

Due to the unexpected effects of lattice relaxation and the corresponding electronic properties we have investigated the role of the xc potential in this context. For this purpose, we have repeated a series of calculations using the local-density approximation (LDA).[30] While the optimal lattice constants obtained with GGA hardly deviate from the experimental ones, LDA yields, as expected, a decrease in the unit-cell volume by 6%. However, the relaxation of the atomic positions shows exactly the same trend as for GGA in terms of the bonding distances. As a consequence, the electronic bands and densities of states obtained by LDA and GGA only differ very little. In both cases, the DOS at the Fermi level vanishes, and also the band dispersions are very similar. Thus, the rather strong impact of computational structure optimization on the bond distances and electronic properties is not sensitive to the choice of the particular xc functional.

In addition, we have used LDA to recalculate the A_g phonon modes for the fully relaxed LDA structure. Due to the smaller unit cell and shorter bond distances in LDA one could expect all phonon frequencies to increase. This is actually the case, with a typical change of 5%–10%. Thus, the GGA results agree clearly better with experiment compared to the ones obtained with LDA.

Having shown that the dramatic changes in the electronic properties upon structural relaxation are not an artifact of the xc functional, but a pure consequence of altered bond lengths within the adopted crystalline symmetry, the reason for these effects still remains unclear. For example, it needs to be clarified whether the experimentally determined space group reflects the symmetry of the stoichiometric unit cell or to which extent, e.g., defects could be responsible for structural distortions. In this context it should be noted that Ming *et al.*[31] recently suggested that the actual structure of NaV_2O_5 is a $1\times2\times1$ crystallographic supercell, where the antiferromagnetic spin exchange gives rise to the insulating gap. This result was obtained by spin-polarized GGA calculations, demonstrating that the main effect for the electronic properties around the Fermi level is not due to strong on-site Coulomb correlations. In view of these findings and considering similar ongoing discussions about the low-temperature phase in NaV_2O_5, the structure solution of the vanadates remains an open issue which asks for further investigations.

VI. CONCLUSIONS

We have studied the electronic, optical, and vibrational properties of MgV_2O_5 from first principles by all-electron FP-APW+lo calculations. We find very pronounced effects of geometry optimization on the bond lengths and, hence, the electronic properties. In particular, the DOS vanishes at the Fermi level, the width of the bonding V $3d_{xy}$ bands is largely increased, and their antibonding counterparts mix with other V 3*d* levels. Based on this band structure we have obtained the diagonal components of the dielectric function in the energy range up to 4 eV. It would be very interesting to compare our calculated results with measured ones as soon as the dielectric function will be experimentally available.[32]

The calculated eigenfrequencies of the A_g phonon modes, together with the Raman spectra, allow a detailed comparison with experimental data and, consequently, an assignment of the measured peak positions in terms of their symmetry

species. Even without taking into account the Hubbard U, we obtained a very good agreement with experimental results, which is a general feature of all ladder compounds we investigated.[22,23] The calculated eigenvectors give a detailed insight into the displacement pattern of each phonon mode. Since the Raman intensities turned out to be quite small for the experimentally used excitation energy, we propose Raman experiments at lower laser energies. In addition, we predict a pronounced resonance of the 546 cm^{-1} mode at 2.7 eV.

ACKNOWLEDGMENTS

The work has been financed by the Austrian Science Fund (FWF) under Project No. P15520. We also appreciate support by FWF under Projects No. P15834 and No. P16227, the EU RTN network EXCITING under Contract HCPR-CT-2002-00317, and the Austrian Academic Exchange Service (ÖAD) WTZ under Project No. 1/2006. E.Y.S. is grateful to the Ikerbasque Foundation and the University of the Basque Country (Grant GIU07/40) for support.

*juergen.spitaler@mu-leoben.at

[1] M. Isobe and Y. Ueda, J. Phys. Soc. Jpn. **65**, 1178 (1996).
[2] M. Weiden, R. Hauptmann, C. Geibel, F. Steglich, M. Fischer, P. Lemmens, and G. Güntherodt, Z. Phys. B: Condens. Matter **103**, 1 (1997).
[3] P. Lemmens, G. Güntherodt, and C. Gros, Phys. Rep. **375**, 1 (2003).
[4] J. Lüdecke, A. Jobst, S. van Smaalen, E. Morré, C. Geibel, and H.-G. Krane, Phys. Rev. Lett. **82**, 3633 (1999).
[5] H. Seo and H. Fukuyama, J. Phys. Soc. Jpn. **67**, 2602 (1998).
[6] M. V. Mostovoy and D. I. Khomski, Solid State Commun. **113**, 159 (1999).
[7] H. Nakao *et al.*, Phys. Rev. Lett. **85**, 4349 (2000).
[8] K. Ohwada, Y. Fujii, Y. Katsuki, J. Muraoka, H. Nakao, Y. Murakami, H. Sawa, E. Ninomiya, M. Isobe, and Y. Ueda, Phys. Rev. Lett. **94**, 106401 (2005).
[9] H. Iwase, M. Isobe, Y. Ueda, and H. Yasuoka, J. Phys. Soc. Jpn. **65**, 2397 (1996).
[10] P. Millet, C. Satto, J. Bonvoisin, B. Normand, K. Penc, M. Albrecht, and F. Mila, Phys. Rev. B **57**, 5005 (1998).
[11] M. Isobe, Y. Ueda, K. Takizawa, and T. Goto, J. Phys. Soc. Jpn. **67**, 755 (1998).
[12] M. A. Korotin, V. I. Anisimov, T. Saha-Dasgupta, and I. Dasgupta, J. Phys.: Condens. Matter **12**, 113 (2000).
[13] M. Onoda and A. Ohyama, J. Phys.: Condens. Matter **10**, 1229 (1998).
[14] P. Millet, C. Satto, P. Sciau, and J. Galy, J. Solid State Chem. **136**, 56 (1998).
[15] M. J. Konstantinović, Z. V. Popovic, M. Isobe, and Y. Ueda, Phys. Rev. B **61**, 15185 (2000).
[16] Z. V. Popović, M. J. Konstantinović, R. Gajić, V. N. Popov, M. Isobe, Y. Ueda, and V. V. Moshchalkov, Phys. Rev. B **65**, 184303 (2002).
[17] H.-J. Koo and M.-H. Whangbo, Solid State Commun. **111**, 353 (1999).
[18] M. A. Korotin, I. S. Elfimov, V. I. Anisimov, M. Troyer, and D. I. Khomskii, Phys. Rev. Lett. **83**, 1387 (1999).
[19] The results differ from those given in Ref. 20 since a bug in the WIEN2K code regarding *CXY* lattices has been fixed, as described in the WIEN2K update info 20 November 2003, under http://www.wien2k.at/reg_user/updates/old_3/index.html
[20] J. Spitaler, E. Y. Sherman, H. G. Evertz, and C. Ambrosch-Draxl, Phys. Scr., T **t109**, 159 (2004).
[21] L. Hozoi, S. Nishimoto, and A. Yamasaki, Phys. Rev. B **72**, 195117 (2005).
[22] J. Spitaler, E. Y. Sherman, H. G. Evertz, and C. Ambrosch-Draxl, Phys. Rev. B **70**, 125107 (2004).
[23] J. Spitaler, E. Y. Sherman, and C. Ambrosch-Draxl, Phys. Rev. B **75**, 014302 (2007).
[24] C. Ambrosch-Draxl, H. Auer, R. Kouba, E. Y. Sherman, P. Knoll, and M. Mayer, Phys. Rev. B **65**, 064501 (2002).
[25] Crystal structures are produced with XCRYSDEN (A. Kokalj, Comput. Mater. Sci. **28**, 155 (2003)); see http://www.xcrysden.org/
[26] E. Sjöstedt, L. Nordström, and D. J. Singh, Solid State Commun. **114**, 15 (2000).
[27] P. Blaha, K. Schwarz, G. K. H. Madsen, D. Kvasnicka, and J. Luitz, *WIEN2k, An Augmented Plane Wave + Local Orbitals Program for Calculating Crystal Properties* (Karlheinz Schwarz, Techn. Universitaet Wien, Austria, 2001) [Improved and updated Unix version of the original copyright WIEN code, which was published by P. Blaha, K. Schwarz, P. Sorantin, and S. B. Trickey, Comput. Phys. Commun. **59**, 399 (1990)].
[28] J. P. Perdew, K. Burke, and M. Ernzerhof, Phys. Rev. Lett. **77**, 3865 (1996).
[29] C. Ambrosch-Draxl and J. O. Sofo, Comput. Phys. Commun. **175**, 1 (2006).
[30] J. P. Perdew and Y. Wang, Phys. Rev. B **45**, 13244 (1992).
[31] X. Ming, H.-G. Fan, Z.-F. Huang, F. Hu, C.-Z. Wang, and G. Chen, J. Phys.: Condens. Matter **20**, 155203 (2008).
[32] Analysis of optical properties of a different family of ladder compounds can be found in S. Yamamoto and J. Ohara, Phys. Rev. B **76**, 235116 (2007).